Carbon Nanofibers Provide a Cationic Rectifier Material: Specific Electrolyte Effects, Bipolar Reactivity, and Prospect for Desalination

Luthando Tshwenya [a], Frank Marken [b*], and Omotayo A. Arotiba [a,c*]

[a] *Department of Applied Chemistry, University of Johannesburg, Doornfontein, 2028, South Africa*

[b] *Department of Chemistry, University of Bath, Bath BA2 7AY, UK*

[c] *Centre for Nanomaterials Science Research, University of Johannesburg, South Africa*

Corresponding authors: F.Marken@bath.ac.uk and oarotiba@uj.ac.za

Abstract

We demonstrate that ionic current rectification effects are observed with a film of negatively charged carbon nanofibers (CNFs) deposited as a film or mat onto a 10 μm diameter microhole in poly-ethylene-terephthalate (PET). CNFs are synthesized via a chemical vapor deposition (CVD) method, followed by oxidation with hydrogen peroxide to introduce carboxyl moieties (providing negative surface charges). Carbon nanofibers are characterized with transmission electron microscopy (TEM), scanning electron microscopy (SEM), elemental analysis, and by zeta potential measurements. When drop-dried asymmetrically onto a 10 μm diameter cylindrical channel on a 6 μm thick PET substrate and placed as membrane between two electrolyte compartments, ionic current rectification is observed. Effects of pH, ionic strength, and nature of electrolyte are investigated. Bipolar reactivity of iodide is demonstrated. Potential for future applications in water purification is discussed.

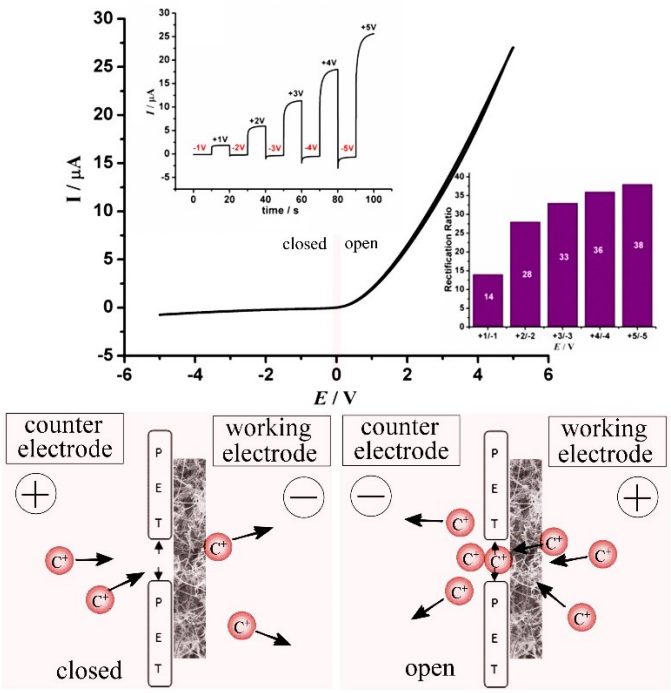

Graphical Abstract

Keywords: carbon nanofiber; voltammetry; membrane; ionic rectifier; desalination

1. Introduction

Ionic rectifier[1] processes inhibit the flow of ions uni-directionally in a similar way to processes in electronic rectifiers or diodes. Ionic rectifier processes have been reported for asymmetric membranes[2,3] and membrane reactions,[4] for nanochannels[5,6] and nanopores,[7] in new materials such as metal-organic frameworks[8] and polymers of intrinsic microporosity,[9] at nanocones and pipettes,[10] and at microholes.[11] Considerable progress has been made by Lei Jiang and coworkers particularly for ionic rectifiers and gates in modified nanopores based on track-etch membranes.[12,13,14,15] In the absence of track-etch nanopores, also semi-permeable materials such as Nafion[16] and graphene oxide[17] can be employed, when deposited asymmetrically onto a cylindrical microhole of 5 to 40 μm diameter and 6 μm length. Voltage-induced compositional changes are observed within the cylindrical microhole region.[16] This can be described as a depletion of ions (in the "closed" diode) and as an accumulation of ions (in the "open" diode) resulting in potential dependent resistance changes. Ionic rectifier processes have been suggested to lead to ionic transistors[18] and "iontronics",[19] but also to new types of sensors[20] and desalination systems based on alternating current driven ion removal.[21]

Materials for ionic rectifiers are based on ionomers and require a degree of semi-permeability in order to induce the potential-dependent resistance changes in the microhole.[16] Rectifier effects have been demonstrated previously for commercial ion exchange membranes,[22] for cellulose,[23] and for 2D-titanate nanosheets.[24] Further candidates could be based in particular on porous surface-charge carrying carbon nanomaterials. Carbon nanofibers provide robust but highly porous films with high surface area[25] and convenient synthesis often based on bio-resources.[26] They are readily obtained with negative surface charge and deposited from suspension into mechanically robust porous films.[27] Carbon nanofibers (CNFs) represent a class of carbon nanomaterials with a fibrous (and sometimes tube-like) structure that is relatively cheap and easy to synthesize.[28] A common synthetic route to CNFs is based on electrospinning of polymer solutions (e.g. poly-acrylonitrile or poly-pyrrole in an organic solvent such as

DMF) followed by carbonization in the presence of inert gas.[29] An alternative route (employed here to give more readily dispersable and processable materials) is the growth of CNFs directly using an oil-catalyst precursor suspension and acetylene-based chemical vapor deposition and carbonization.[30]

Carbon nanofibers have received much attention due to their potential for application in wearable nano-electronics,[31] as electrode materials for electrochemical capacitor cells and sensors,[32] as electrocatalyst support,[33] in rechargeable batteries,[34] etc. When made into films or fibrous mats via suspension deposition, CNFs align themselves irregularly forming mechanically robust entangled networks with open porous channels that can serve as pathways for ion flow. Semi-permeable behaviour can be induced by chemically introducing negative surface charges.

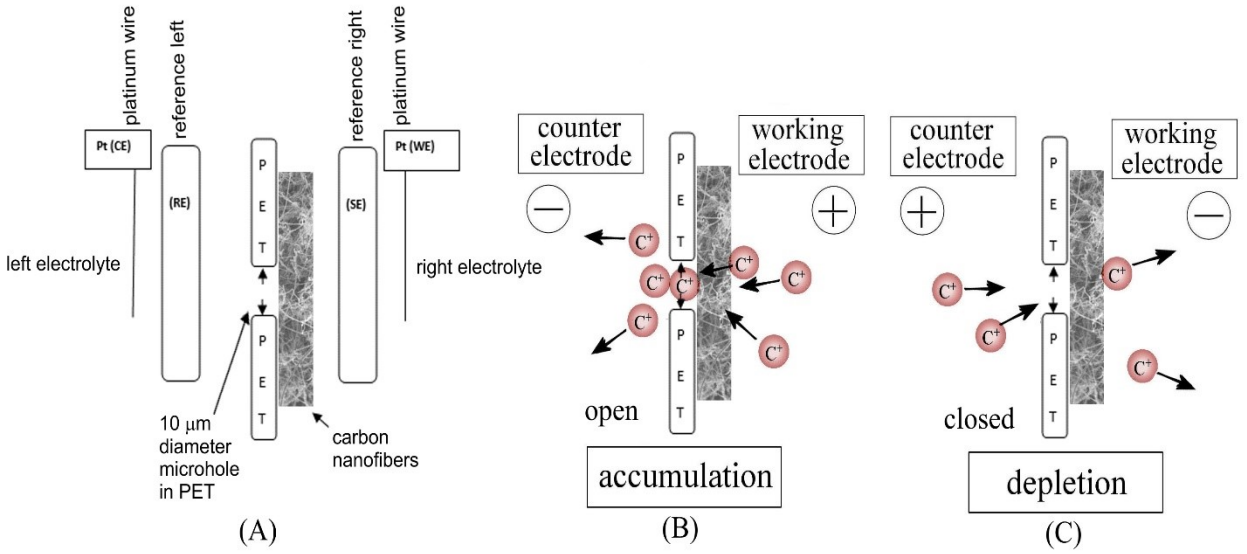

Figure 1. (A) Illustration of the ionic rectifier experiment with four-electrode potential control across a PET film with microhole. Carbon nanofibers are deposited on one side (the working electrode, WE) to create a semi-permeable cation conduction region. (B) Schematic depiction of the open diode with cations/salt accumulating in the cylindrical microhole under positive bias. (C) Schematic depiction of the closed diode with cations/salt depleting from the cylindrical microhole under negative bias.

In this study, we synthesize carbon nanofibers for application in ionic rectifiers. The carbon nanofibers are surface-oxidized to provide cation conducting porous networks. Figure 1A shows the experimental system for membrane electrochemistry with carbon nanofibers asymmetrically applied as a film or mat to a 10 μm diameter microhole in at 6 μm thick poly-ethylene-terephthalate (PET) film. A standard four-electrode potentiostat system is employed to apply a well-defined voltage across the CNF membrane. When placed between electrolyte solutions with the carbon nanofiber film facing the working electrode, cationic diode behavior is observed. This is because of the interaction of cations travelling within the negatively charged nanofiber film. Effects of the type of electrolyte, the concentration, and the pH are reported. In spite of the highly open porous structure of carbon nanofibers, there is potential for future application in ionic rectifier based desalination systems.

2. Results and Discussion

2.1. Characterization of Carbon Nanofiber Elemental and Surface Properties

In order to determine the morphology and thickness of the carbon nanofibers film/mat, scanning electron microscopy (SEM) imaging was employed. A carbon nanofiber dispersion was deposited on a substrate (a glass slide) lifted off, and then placed vertically on a carbon tape coated chamfer/cross-section specimen stub, with the edge of the carbon nanofibers deposit/film slightly protruding from the carbon tape and stub. Figure 2A shows a side view image of the carbon nanofiber film as well as the typical film thickness, about 26 μm. Figure 2B shows the front view of the film, as well as the irregular arrangements of the carbon nanofibers in the deposit. The carbon nanofibers appear long and irregular in size as a result of pulverizing and sonication, which caused the breaking of some into shorter fibers.

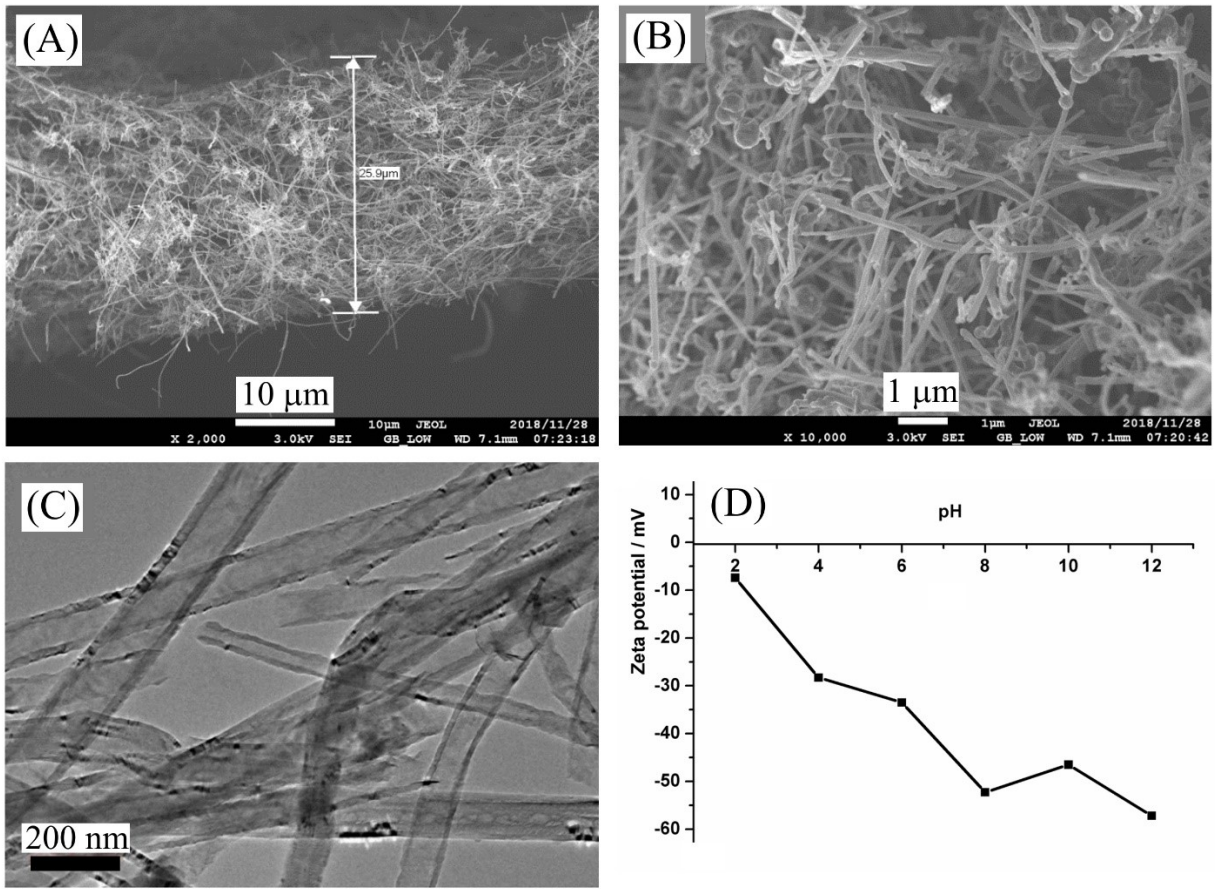

Figure 2. Scanning electron microscopy images showing (A) the thickness and cross-section and (B) the general carbon nanofiber morphology for a film deposit. (C) Transmission electron micrograph for carbon nanofibers. (D) Zeta potential data from measurement for nanofibers (approx. 0.2 mg/cm^3) dispersed in aqueous electrolyte solution (pH adjusted with HCl and NaOH).

HR-TEM studies (Figure 2C), confirm that the carbon nanofibers synthesized in this work indeed have an open architecture, comprising of interior (hollow core) and exterior (wall) surfaces. The synthesis results in long, irregular nanofibers with an average diameter of about 105 nm. Energy dispersive spectroscopy (EDS) results indicate the presence of carbon (90 atom %), oxygen (8.6 atom %), and iron (1.1 atom %). These are consistent with the carbonization and oxidation steps applied during the synthesis.

To confirm success of the oxidation step and to determine the overall surface charge of the carbon nanofibers, zeta potential measurements were conducted. Here, a small amount of carbon nanofibers (0.2 mg/cm^3) was suspended with ultrasound in water at

different pH values (adjusted to pH 2-12). Figure 3D shows that the carbon nanofibers retain a negative surface charge throughout the pH range, with a point of zero charge probably between pH 1 and 2. A negative surface charge is important for semi-permeable characteristics resulting in cation conduction. The pore sizes and charge density in the carbon nanofiber mat are important in maintaining semi-permeability at higher ionic strengths. However, as will be shown below, further optimization of these parameters will be possible in the future.

2.2. Characterization of Electrochemical Membrane Properties

Figure 3A summarizes the experimental system for the measurement of ionic currents through the membrane. Figure 3B shows ionic current data from steady state cyclic voltammograms obtained in aqueous 10 mM NaCl (both sides). For the empty microhole in PET only resistive characteristics are observed without any sign of rectification (black line). However, with the CNF film deposit a dramatic change occurs (red line). In the positive potential range a resistance decrease (higher current) is observed and in the negative potential range a resistance increase (lower current) is seen. This type of characteristic is consistent with a cationic diode with cations dominating the ionic current. For this case, Figure 1B describes the case of electrolyte accumulation leading to low resistance with a positive potential applied to the working electrode. In contrast, Figure 1C illustrates the case of negative applied potential with electrolyte depletion in the microhole region resulting in high resistance. The observations are in agreement with the highly porous CNF material exhibiting negative surface charge and therefore resulting in at least partial semi-permeable behaviour and cation transport.

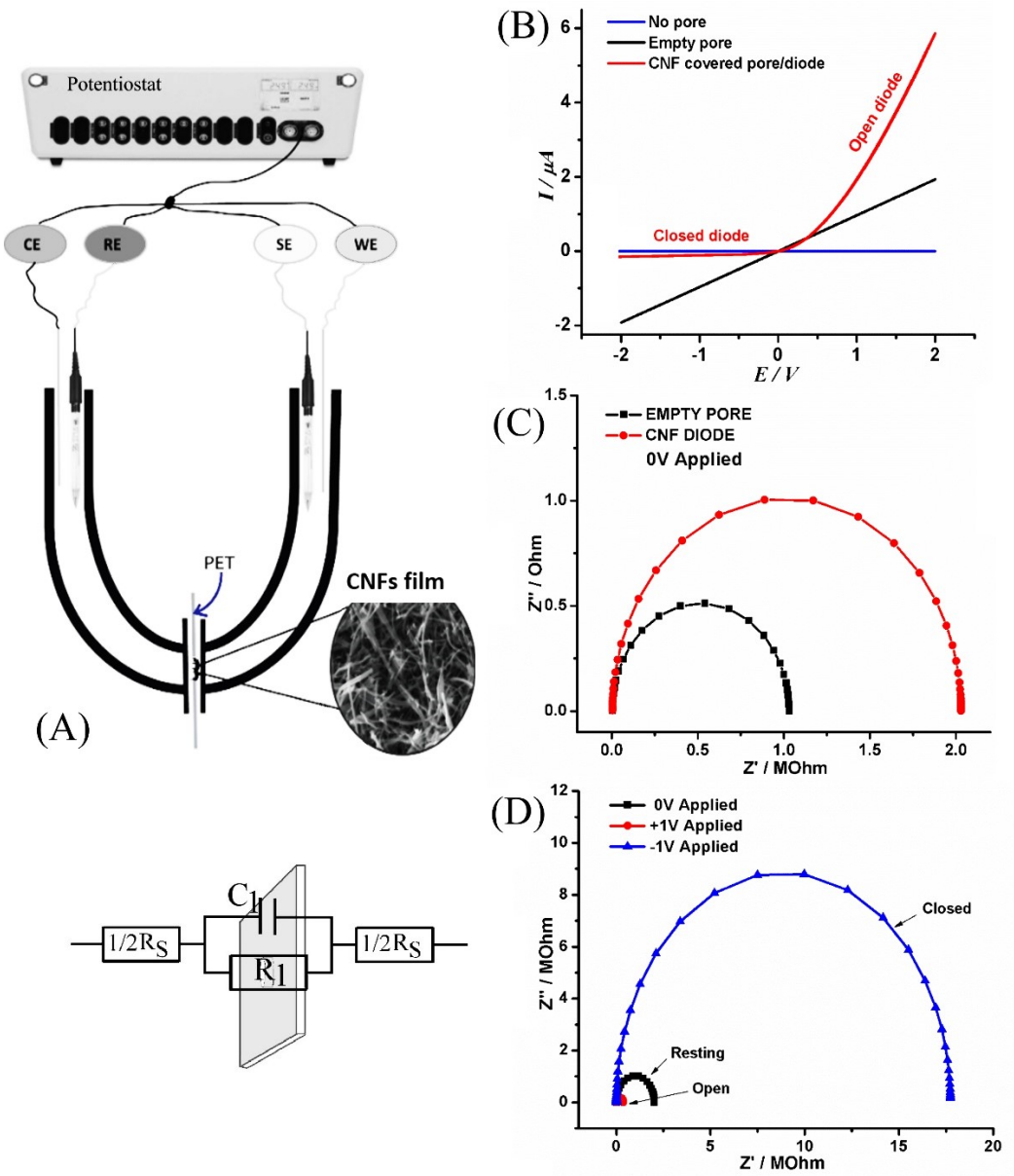

Figure 3. (A) Electrochemical setup with an asymmetric deposit of CNFs on a 10 μm pore on PET, (B) Cyclic voltammograms in 10 mM NaCl (at 20 mV s^{-1}) for a PET with no microhole (blue), an empty 10 μm microhole (black) and CNF covered 10 μm diameter microhole. (C) Nyquist plots for impedance data (consistent with a [R(RC)] equivalent circuit, see illustration) for an empty microhole (black) and for an asymmetric deposit of CNFs (red), when 0.0 V is applied with 100 mV amplitude. (D) Nyquist plots showing the effect of bias voltage on ion flow for a cylindrical 10 μm microhole asymmetrically covered with CNFs.

Further experiments are performed with electrochemical impedance spectroscopy. Figure 3C shows data comparing the impedance response for the empty microhole and for the CNF coated microhole. At an applied bias of 0.0 V a significant difference is observed with both systems resulting in a well-defined semicircle. Figure 3D shows data for the

CNF coated microhole comparing a bias voltage of +1 V (open diode; 0.3 MOhm), 0 V, and -1 V (closed; 17 MOhm). Table 1 gives a summary of EIS data (for the equivalent circuit fit) where R_S represents solution resistance in the bulk and in the microhole vicinity. The element C_1 represents PET interfacial capacitance and remains constant at 0.6 to 0.9 nF in all conditions. R_1 is linked with PET polarization upon asymmetric introduction of the carbon nanofiber film (both the CNF film resistivity and electrolyte influence this element). This resistance element appears to be drastically affected by potential bias and this is attributed here to accumulation (+1 V) and depletion (-1 V) of electrolyte within the microhole. The actual switching of the diode does take place on a second time scale (or in 1 Hz frequency domain) and is therefore not directly observed at the frequencies applied here.

Table 1. EIS data for an empty pore, a CNF coated 10 µm diameter microhole (CNF ionic diode) at 0 V applied bias, as well as data when the diode is "open" (+1 V bias) and "closed" (-1 V bias). The frequency range is from 100 KHz to 100 Hz, amplitude 100 mV. Only the high frequency semicircular part of the Nyquist plot data is analysed. Although data fits are excellent, device-to-device variation and errors are estimated typically ± 30% mainly due to variation in CNF film.

Conditions	**R_S / KOhm**	**R_1 / MOhm**	**C_1 / nF**
Open pore vs. CNF coated pore (0 V applied)			
Open pore	4.37	1.03	0.73
CNF diode	4.57	2.03	0.58
CNF diode (different applied voltages)			
0 V	4.57	2.03	0.58
+1 V	4.20	0.37	0.57
-1 V	4.10	17.7	0.87

Effect of Increasing the Potential Window. The influence of applied potential on the ionic current rectification was studied in aqueous 10 mM NaCl (Figure 4). The current in the positive potential window increases rapidly to a maximum of 27 µA at 5 V. When the

potential bias is reversed, the current stays close to zero apart from some increase in current especially at potentials negative of -2 V (attributed previously to the over-limiting potential region, where convective processes occur [16]). A summary of the rectification ratio as a function of applied potential is shown as a bar graph in Figure 4C. With higher applied bias, clearly higher rectification effects are seen with a ratio of open to closed ionic current of up to 38 at +/-5 V.

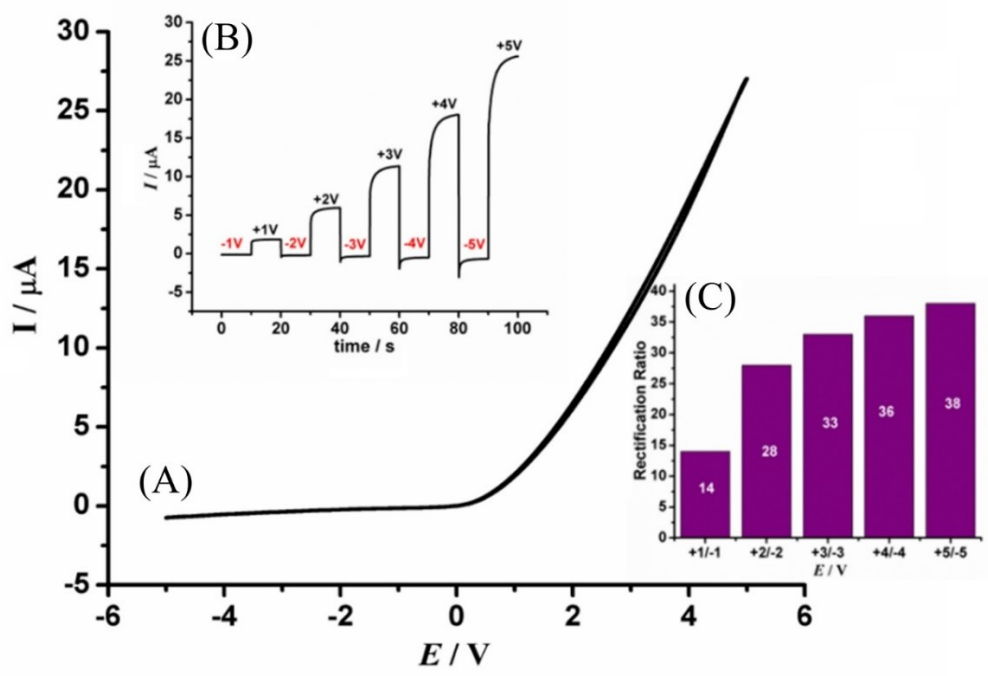

Figure 4. (A) Cyclic voltammetry responses (with inserts of (B) chronoamperometry responses and (C) rectification ratio bar plot when voltage is stepped from ±1 V to ±5 V) for a carbon nanofiber based ionic diode exposed to a 10 mM NaCl solution (both sides).

Effects of Electrolyte Nature and pH. Voltammetry data were obtained for CNF diodes in 10 mM NaCl, in acidic 10 mM HCl, and in alkaline 10 mM NaOH. Figure 5 shows data for a +/-2 V potential window. For all three cases cationic diode behaviour is observed consistent with the more acidic PZC for CNFs resulting in anionic surface charges and

cation conduction. Significant differences are seen in the current in the closed state (in the negative potential range) where 10 mM NaCl shows better rectification. In the presence of NaOH, some instability is observed (possibly due to CNF material getting dislodged). In the presence of 10 mM HCl generally higher currents are detected (protons exhibit significantly higher diffusion rates), but the rectification effect is less pronounced. This could be attributed to the lower negative surface charge on the CNF material at this pH.

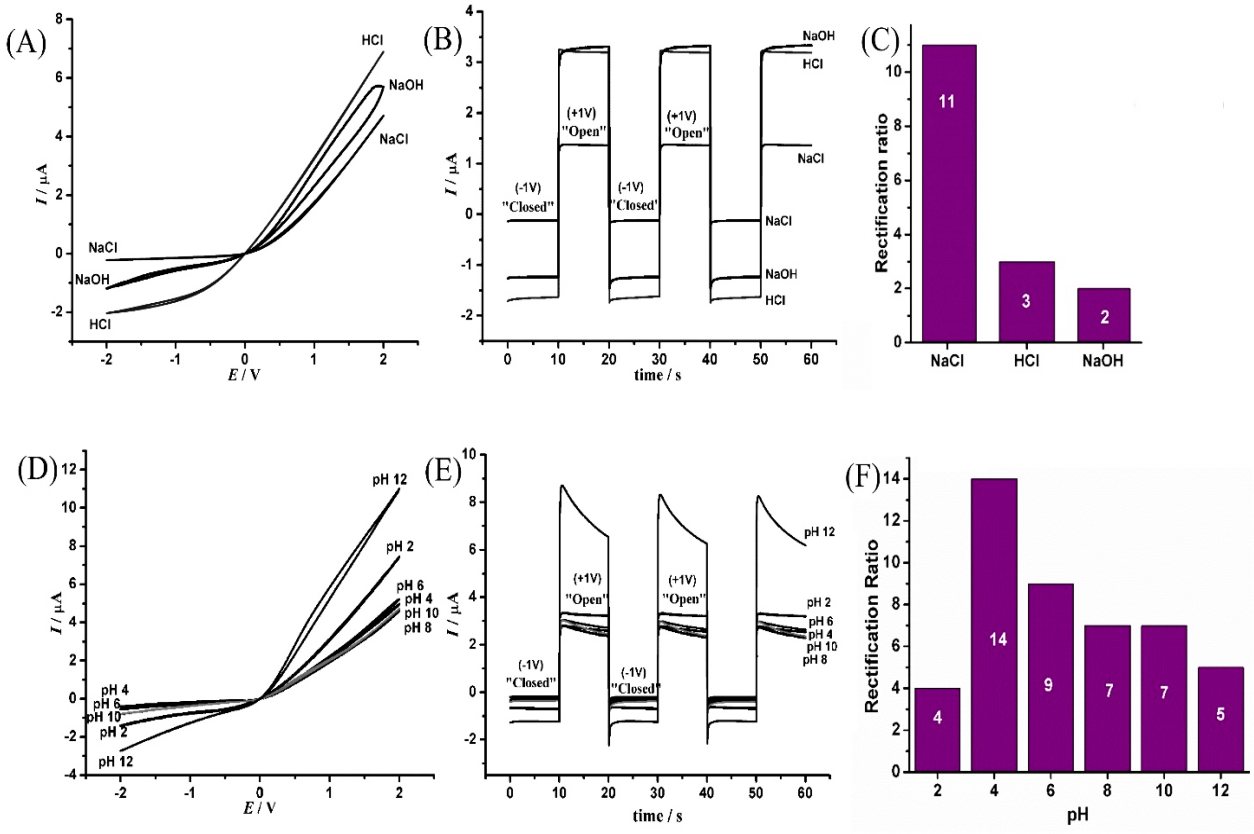

Figure 5. Data for asymmetric carbon nanofiber deposits. (A) Cyclic voltammograms (scan rate 2 mV s^{-1}), (B) chronoamperometry data (stepping from + 1 to − 1 V), immersed in aqueous NaCl (black), HCl (red), NaOH (blue) along with (C) rectification ratio data. (D) Cyclic voltammograms (scan rate 2 mV s^{-1}), (E) chronoamperometry data (stepping from + 1 to − 1 V), 10 mM NaCl at different pH values (adjusted with HCl and NaOH). (F) Rectification ratio data.

Chronoamperometry (Figure 5B) was employed to quantify current rectification at +/-1V. A bar plot in Figure 5C summarizes the data. Clearly, in the presence of aqueous NaCl

the best rectification effects are observed (although overall currents are lower) and therefore sea water desalination based on the rectification process could be possible with CNF materials. The time scale for diode switching is relatively fast (< 1s) indicative of an approach to steady state within a second, which is consistent with previous reports.[16] Clearly, pH plays a significant role in the rectification process and on the stability of carbon nanofiber film based ionic diodes. Figure 5D shows the effect of systematically varying the pH of a 10 mM NaCl solution. I-V curves and chronoamperometry data suggest that the best performance of the diode can be achieved close to the neutral pH range.

Effects of Ionic Strength. The effect of ionic strength was studied by systematically varying the concentration of sodium chloride from 1 mM – 100 mM NaCl and by using the carbon nanofibers deposited onto a PET film with a 10 μm diameter microhole. Unless otherwise stated, the two compartments of the electrochemical cell were symmetrically filled with aqueous NaCl of the same ionic strength. Figure 6A demonstrates a gradual increase in “open” state currents upon increasing the concentration of NaCl. Similarly, currents in the closed state (in the negative potential window) increase. The increase in current in the positive potential window is linked to enhanced cation conductivity at higher concentration. In the negative potential range depletion occurs and currents remain low. At higher ionic strength, the ionic current increase in the negative potential region can be attributed to loss of semi-permeability at higher salt concentrations. The highest rectification effect is observed for 1 mM NaCl (see Figure 6B and 6C). For seawater solution with approximately 0.5 M NaCl the observed rectification effects would be too low to develop desalination methods. Therefore, in future the pore size and/or charge density of the CNF material will have to be changed so that semi-permeable behaviour can be maintained even at higher ionic strengths.

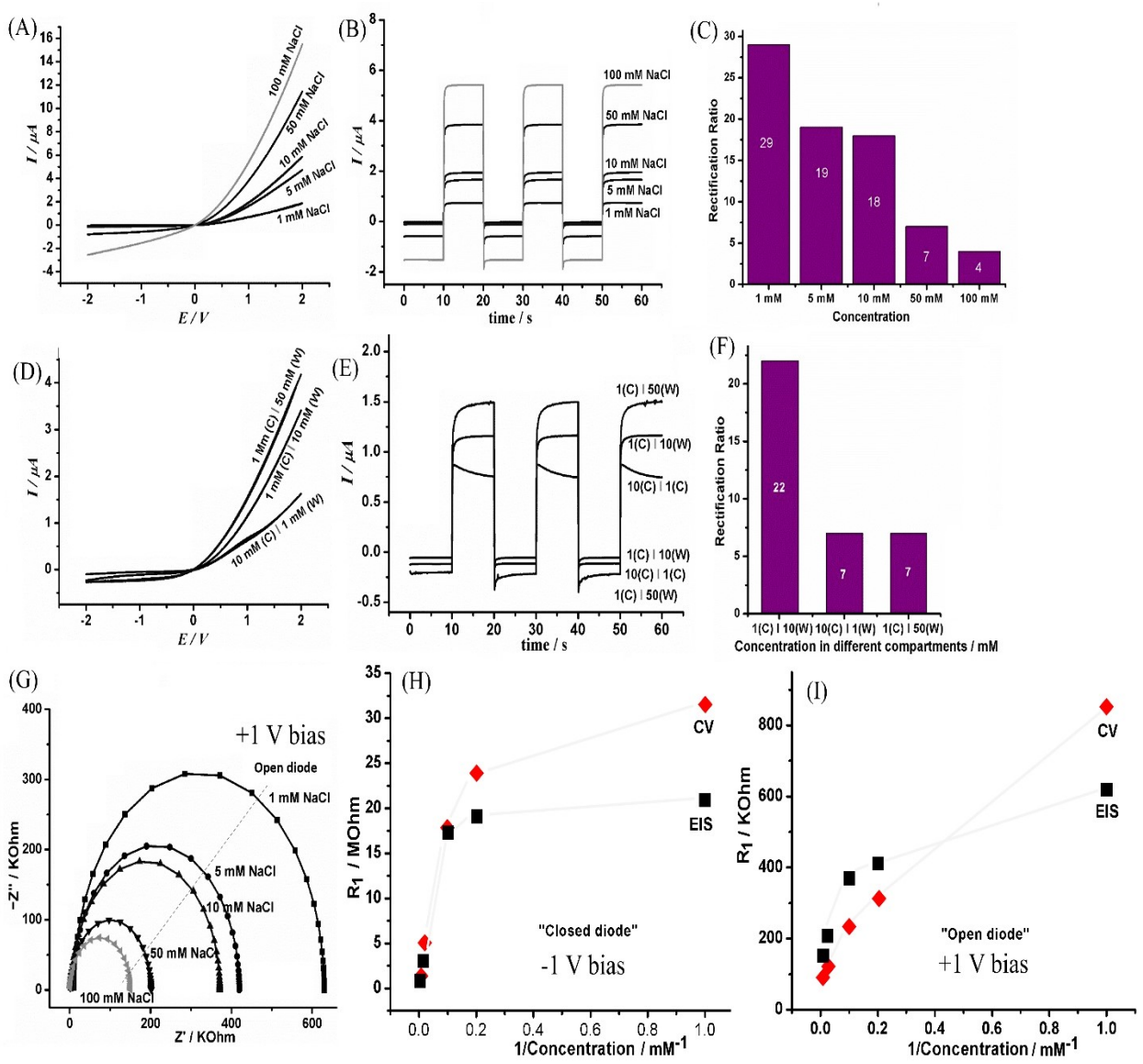

Figure 6. (A) Cyclic voltammograms, scan rate 20 mVs^{-1} for a NaCl concentration of 1, 5, 10, 50, and 100 in mM. (B) Chronoamperometry data stepping from +1 V to -1V. (C) Plot of the rectification ratio (the absolute of the current at +1 V divided by the current at -1 V) *versus* concentration. (D) Cyclic voltammograms (scan rate 20 mV s^{-1}) with 1 mM NaCl in the counter electrode compartment and 10 mM NaCl in the working electrode compartment, or *vice versa*, and for 50 mM NaCl in the working electrode compartment and 1 mM NaCl is in the counter electrode compartment. (E) Chronoamperometry data stepping from +1 V to -1V for asymmetric concentration in working (W) and counter (C) electrode compartments. (F) Bar plot of the rectification ratio. (G) Nyquist plot showing the effect of concentration on the open state of the diode (+1V applied bias). (H) Resistance data obtained from cyclic I-V curves *versus* data from EIS when diode is closed (-1V). (I) Resistance data for the open diode (+1V).

The performance of the ionic diode was also investigated for cases in which the electrolyte concentration varied between left and right half cells. The performance of the diode under

these asymmetric conditions could be important with future applications in desalination in mind. Figure 6D shows data for the case of 10 mM NaCl in the working electrode compartment and 1 mM NaCl in the counter electrode compartment. This is contrasted to the case of 1 mM NaCl in the working electrode compartment and 10 mM NaCl in the counter electrode compartment. A much enhanced rectification ratio of approximately 22 was obtained when a high concentration of NaCl was in the working electrode compartment with counter electrode compartment containing less Na^+ and Cl^- ions. This observation is consistent with cations being readily “pumped” from the high concentrated (working electrode) side into the side with less NaCl (counter electrode). Increasing the concentration on the side of the working electrode drastically decreases the rectification ratio. This result implies that for desalination applications, where the salt concentration is enriched in one compartment and depleted in the other, the rectification ratio needs to stay high up to 1 M NaCl.

Electrochemical impedance spectroscopy (EIS) can be used to assess and disect the resistance to ion flow, when different potentials are applied to the CNF film asymmetrically covering a 10 μm cylindrical hole on a PET substrate.[16] Figure 6G shows data as a function of NaCl concentration. As expected, both the forward (open state) and reverse (closed state) resistances to ion flow increases inversely proportional to NaCl concentration (Figures 6G and 6I). However, the data plots are non-linear. Data from both CV and EIS show similar trends. At lower concentration of NaCl the resistance plateaus probably due to the difference of electrolyte depletion and electrolyte accumulation becoming less relevant.

Table 2 gives the summary of EIS data. When analyzing the EIS elements (R_S - solution resistance, R_1 - resistance associated with carbon nanofibers film and electrolyte resistivity within the microhole region, as well as C_1 - the PET film capacitance) that contribute to the semicircular feature of the Nyquist plot as concentration is varied, several observations can be noted. As expected, R_S decreases with an increase in concentration, but the magnitude remains relatively the same for both the open and closed states of the

cationic diode. C_1 remains almost constant (± 0.5 nF) for all the electrolyte concentration during the open state of the diode, but is slightly influenced (although not much) by a negative potential bias. R_1 decreases with an increase in concentration in both the open and closed states of the diode, but more resistance is to cation flow is experienced during the closed state of the diode especially for lower concentrations. The data suggests that the concentration of the electrolyte plays a significant role on diode performance, as well as on the conductivity of the CNF ionic diode. An alternative measure of the rectification ratio can be obtained from $R_{1,closed}/R_{1,open}$ = 33, 46, 48, 14, 4.8 for concentrations of 1, 5, 10, 50, and 100 mM, respectively. This is almost consistent with data in Figure 6C.

Table 2. Summary of EIS data for different concentrations of NaCl for a CNF film on a 10 μm diameter microhole, during the "open" and "closed" states of the ionic diode (frequency range 100 kHz – 100 Hz, amplitude 100 mV, only the high frequency semicircular part of the Nyquist plot data is analysed; device-to-device errors were less 10% except for operation during the closed state (-1 V bias, and low concentrations) where errors up to 30% are experienced).

concentration	**R_S / KOhm**	**R_1 / MOhm**	**C_1 / nF**
Bias +1.0 V (open diode)			
1 mM	9.54	0.62	0.46
5 mM	7.01	0.41	0.52
10 mM	4.20	0.37	0.57
50 mM	1.16	0.20	0.57
100 mM	0.61	0.15	0.57
Bias -1.0 V (closed diode)			
1 mM	8.68	20.8	0.58
5 mM	6.86	19.0	0.89
10 mM	4.10	17.7	0.87
50 mM	1.22	2.77	0.63
100 mM	0.67	0.72	0.59

Effect of Different Cations and Anions. Specific interactions between cations or anions and the carbon nanofiber material are possible. In particular, interactions that change the characteristics of the ionic diode response could be of interest. Figure 8A shows data for the steady state cyclic voltammetry responses in the presence of aqueous 10 mM NaCl, KCl, LiCl, $CaCl_2$, and $AlCl_3$. Although generally following the pattern of cationic diode behaviour, there are significant changes in rectification. KCl produces the highest current in open state, but based on chronoamperometry data, lithium, sodium, and potassium cations produce similar characteristics. For $CaCl_2$ a lower rectification is observed possibly due to both the higher ionic strength and some binding to CNFs. A dramatically different behaviour is observed for $AlCl_3$ and this can be attributed to a specific interaction with Al^{3+} binding to the negatively charged CNF surface. Only resistive behaviour is seen and there is no evidence for rectification (Figure 7C).

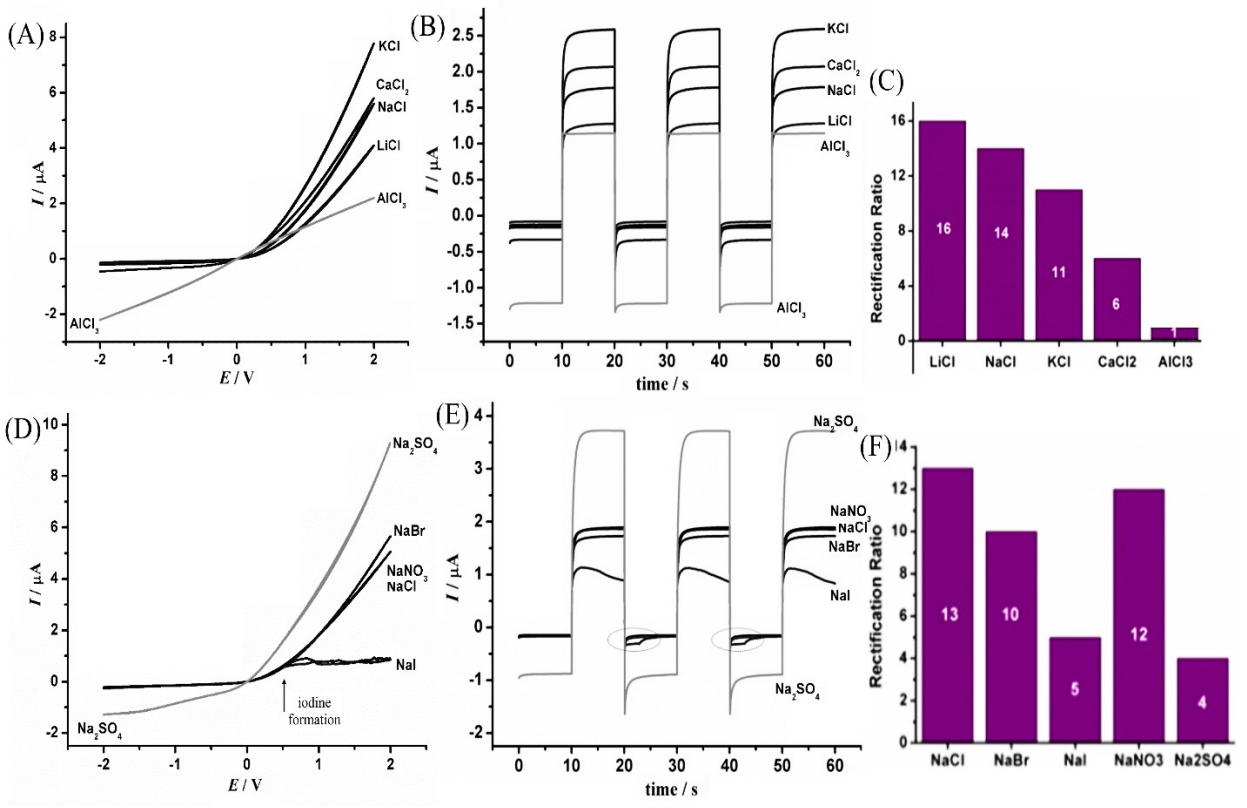

Figure 7. (A) Cyclic voltammograms (scan rate 20 mVs^{-1}; 10 mM solution on both sides) showing the effect of different cations in the electrolyte. (B) Chrono-amperometry data along with (C) a bar graph with

rectification ratio data when a CNF diode is immersed in different solutions containing different cations. Data for different anions are shown in (C) and (D) and (F).

Even more intriguing is the cationic diode behaviour for sodium salt of different types of anions (see Figure 8D). Anions of mono-valent and di-valent nature (Cl^-, Br^-, I^-, NO_3^- and SO_4^{2-}) are investigated. Clearly, the di-valent sulfate lowers the rectification ratio (see Figure 7F). Chloride, nitrate, and bromide exhibit very similar characteristics. However, the most interesting feature is observed for iodide. This is the only anion for which the "open" diode state is blocked. At a potential of approximately +0.7 V the current plateaus without further increase even up to 2 V. This behaviour is specific to iodide and explained here based on the bipolar reactivity of the CNF membrane (see Figure 8).

In order to better understand the bipolar reactivity in this CNF membrane, the different types of charge carriers need to be discussed. When a negative potential is applied at the working electrode, cations are driven towards the right, but anions as well as electrons in the carbon material are driven to the left. Figure 8 illustrates this for (A) cation depletion, a closed diode state, and CNF membrane charging as indicated by δ+ and δ-. In (B) for inverted polarity, accumulation of cations and anions in the microhole cause an open state of the diode and δ+ and δ- are also inverted. Iodide anions are accumulated and locally oxidized at the CNF membrane. The internal transport of electrons is then responsible for oxidation of iodide within the microhole to give tri-iodide or iodine (which strongly binds to carbon surfaces[35]). At this stage, it is not fully resolved whether KI_3 (aqueous solubility relatively high) or I_2 (aqueous solubility relatively low with 1.13 mM at 20 ^oC[36]) is the main cause for the diode blocking. However, the mechanism appears to be specific to iodide and it appears to be based on bipolar reactivity at the CNF membrane. This bipolar reaction effectively closes the diode and inhibits the ionic current flow. In future, this phenomenon could be employed also for the analytical detection of iodide.

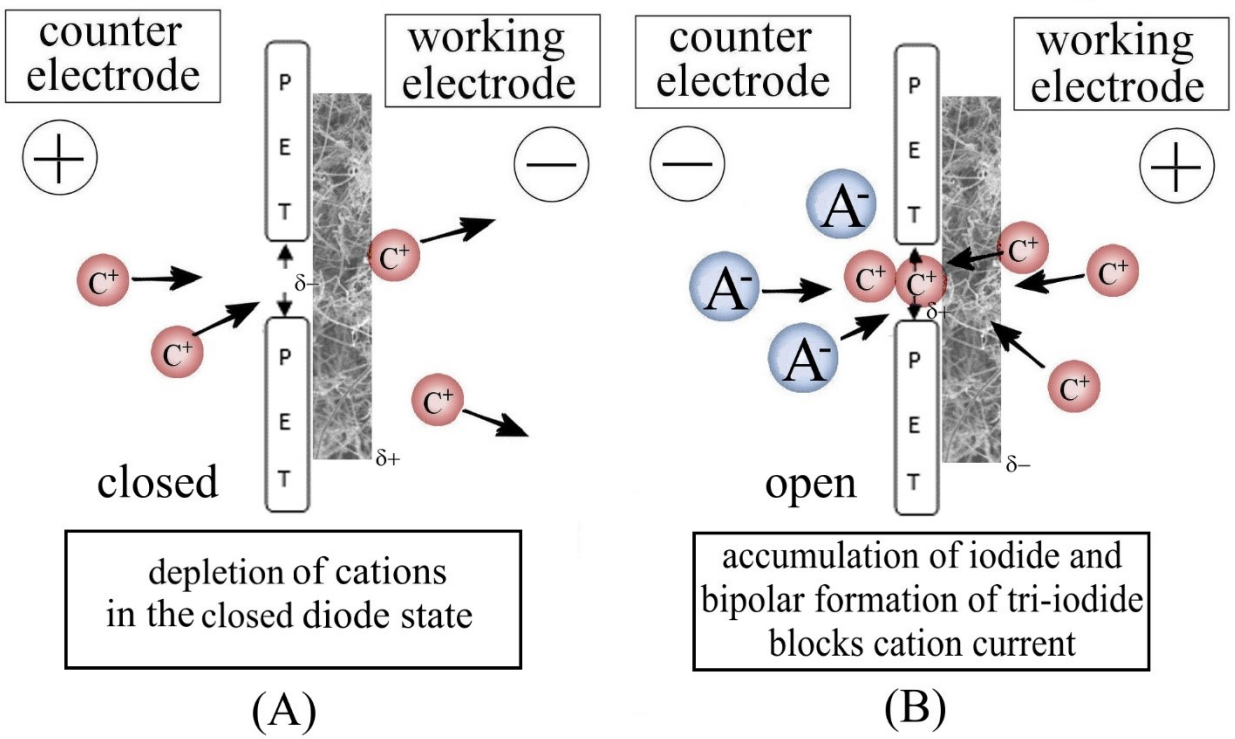

Figure 8. Schematic drawing of (A) the cation flow and accumulation for the closed diode (with negative applied potential at the working electrode) and (B) the corresponding illustration of the open diode (positive applied bias) with anion accumulation in the microhole. For the case of iodide this lead to "bipolar" oxidation and formation of triodide/iodine in the microhole. This blocks/closes the diode chemically and limits the current.

3. Conclusions

It has been shown that carbon nanofiber materials can be useful as semi-permeable films or mats in ionic current rectifiers. The negative surface charge (induced by oxidation with H_2O_2) allows cationic diode or rectifier phenomena to be observed. The most pronounced rectification effects are detected at low ionic strength and at neutral pH (consistent with the double layer induced by the surface charge causing the effects). For applications in desalination, salt levels of 0.1 M could be treated, but actual salt levels in seawater are too high for this particular type of CNF to work effectively. Optimization parameters to consider are the porosity and pore size of CNF materials, charge density, the PET microhole diameter/length, and the thickness of CNF mat. For realistic desalination prospects also multi-microhole arrays will be required. Improved CNF materials are accessible when the density of the CNF film is increased, pore sizes are lowered, and the

thickness is increased. More work on related materials will be necessary to further develop this application and to explore further benefits from the relatively open pore structure when compared to traditional desalination membranes.

Specific cation effects due to interactions with CNFs are detected particularly for Al^{3+} binding causing a loss of rectification. The presence of Al^{3+} is most sensitively detected in the negative potential range for the “closed” diode when Al^{3+} causes a strong increase in current. Specific anion effects have been identified for iodide. A bipolar redox process has been proposed to be responsible for a chemical blocking of the CNF diode. This process relies on the electronic conductivity of CNFs and it can lead to iodine formation as a water-insoluble product physically blocking ion transport through the CNF film. Time constants for the diode opening/closing response have been compared to the much slower iodine blocking/unblocking reaction.

In the future, CNF materials have to be improved by increasing surface charge and by increasing density (smaller pore diameter to maintain semi-permeable conditions even at higher ionic strengths). This could be achieved by densification e.g. pressing, or by synthesis of a more dense and more branched CNF material. Bipolar redox reactions within ionic diodes are entirely new and represent a first example of coupling ionic current and electronic current flow in a bipolar nanofluidic membrane rectifier process.

4. Experimental Section

4.1. Materials

The laser-drilled polyethylene terephthalate (PET) films used in this work were purchased from Laser Micromachining Limited (Birmingham, United Kingdom). Salts and solvents used were of high purity and were purchased from Sigma Aldrich (South Africa). Ultrapure water for electrolyte solutions (18.2 MOhm cm at 22 ^{o}C) was prepared in-house using a Milli-Pore system (South Africa).

4.2. Carbon Nanofibers Synthesis

Carbon nanofibers were synthesized using a method initially developed by Suriani et al.[37] Natural oil (derived from chicken fat) was used with 5 wt% of ferrocene catalyst added, dispersed by sonication for 30 min and stirring for another 30 min to achieve complete homogeneity. A clean silica boat substrate was then half-filled with the oil catalyst solution and heated to 470 ºC for 60 min to achieve complete vaporization of volatiles and stabilization of a solid pre-catalyst. Further heating at 650 ºC was carried out in a nitrogen and acetylene-rich atmosphere (acetylene 120 dm^3/min and nitrogen 400 dm^3/min) for 60 min to achieve carbonization (carbon nanofiber synthesis). After cooling to room temperature, the black residue was pulverized, and washed several times with deionized water and then dried at 80 ºC overnight in an oven. To oxidize the carbon nanofibers, 500 mg of the dried sample was refluxed in hydrogen peroxide (30% in water) for 2 h, followed by filtration and drying at 120 ºC for 4 h.

4.3. Ionic Diode Fabrication

A 1 w/v % carbon nanofibers-DMF dispersion was prepared by sonication of 10 mg carbon nanofibers in 1 mL DMF (for 10 min) using an ultrasonic bath. Then, about 10 µL of the dispersed solution was deposited onto a single side of a PET film, exactly where a 10 µm microhole is located. Prior to this deposition, the PET film was placed onto a glass slide that was previously coated with a thin film of 1 % agarose gel to prevent the carbon nanofiber suspension liquid from entering/crossing the microhole. Using a glass rod, the fiber deposit was distributed to form a uniform film on the microhole (with typically 25 to 30 µm thickness, *vide supra*). The assembly comprising of the CNF deposit and PET on a glass slide was placed in a desiccator to dry overnight. Prior to use, the film was rinsed twice with deionized water and once with electrolyte solution.

4.4. Instrumentation

The ionic transportation properties of the carbon nanofibers based ionic diode were studied by measuring current−voltage (I−V) curves, chronoamperometry responses, and electrochemical impedance spectroscopy data using a PGSTAT 302N potentiostat (AUTOLAB). The PET film with the carbon nanofiber film deposit was mounted between two electrolyte chambers (half-cells, see Figure 1A) filled with electrolyte solution. The cell voltage was applied across the membrane in a conventional 4-electrode configuration.[16] The carbon nanofiber film was positioned to face the working (WE) and sense electrodes (SE), while the backside of the PET faced the counter (CE) and reference electrode (RE). The reference and sense electrodes were both Ag/AgCl (1M KCl) electrodes, while the working and counter electrodes were Pt wires. A scan rate of 20 mVs^{-1} was used throughout.

Transmission electron microscopy (TEM) studies were performed on a JOEL JEM 2100, operated at 200 kV. Scanning electron microscopy (SEM) imaging, cross-sectioning and EDS elemental analysis was performed on a JOEL FESEM 7500F instrument coupled with electron dispersive spectroscopy (EDS), using a 12.7 mm diameter, 45/90º chamfer specimen stub, to allow film thickness measurements. This was done by depositing the carbon nanofiber film on a glass substrate, and carefully lifting off the film and mounting (vertically) on a carbon coated adhesive stub, with the film slightly protruding. Surface charge was studied using a Malvern Zeta-sizer (Malvern, South Africa).

Acknowledgements

The authors hereby thank Mr Ludwe Sikeyi and Dr NW Maxakato for providing us with carbon nanofiber samples. L.T. thanks the Global Excellence and Stature, University of

Johannesburg for Doctoral Scholarship. DST/Mintek Nanotechnology Innovation Centre, University of Johannesburg, South Africa; the Water Research Commission (Grant number: K5/2567), South Africa and the National Research Foundation (CPRR Grant numbers: 98887 and 118546), South Africa are acknowledged for their financial support.

References

[1] B. Lovrecek, A. Despic, J.O.M. Bockris, *J. Phys. Chem.* **1959**, *63*, 750–751.

[2] X.D. Huang, X.Y. Kong, L.P. Wen, L. Jiang, *Adv. Functional Mater.* **2018**, *28*, 1801079.

[3] Z. Zhang, L.P. Wen, L. Jiang, *Chem. Soc. Rev.* **2018**, *47*, 322–356.

[4] R. Zhao, G.H. He, Y.L. Deng, *Electrochem. Commun.* **2012**, *23*, 106–109.

[5] H.C. Zhang, Y. Tian, L. Jiang, *Nano Today* **2016**, *11*, 61–81.

[6] W. Guo, Y. Tian, Y, L. Jiang, *Acc. Chem. Res.* **2013**, *46*, 2834–2846.

[7] J. Experton, X.J. Wu, C.R. Martin, *Nanomaterials* **2017**, *7*, 445.

[8] E. Madrid, M.A. Buckingham, J.M. Stone, A.T. Rogers, W.J. Gee, A.D. Burrows, P.R. Raithby, V. Celorrio, D.J. Fermin, F. Marken, *Chem. Commun.* **2016**, *52*, 2792–2794.

[9] E. Madrid, Y.Y. Rong, M. Carta, N.B. McKeown, R. Malpass-Evans, G.A. Attard, T.J. Clarke, S.H. Taylor, Y.T. Long, F. Marken, *Angew. Chem. Int. Ed.* **2014**, *53*, 10751–10754.

[10] W.J. Lan, M.A. Edwards, L. Luo, R.T. Perera, X.J. Wu, C.R. Martin, H.S. White, *Acc. Chem. Res.* **2016**, *49*, 2605–2613.

[11] Y.Y. Rong, Q.L Song, K. Mathwig, E. Madrid, D.P. He, R.G. Niemann, P.J. Cameron, S.E.C. Dale, S. Bending, M. Carta, R. Malpass-Evans, N.B. McKeown, F. Marken, *Electrochem. Commun.* **2016**, *69*, 41–45.

[12] Q. Liu, K. Xiao, L.P. Wen, H. Lu, Y.H. Liu, X.-Y. Kong, G.H. Xie, Z. Zhang, Z.S. Bo, L. Jiang, *J. Amer. Chem. Soc.* **2015**, *137*, 11976–11983.

[13] Z. Zhang, X.-Y. Kong, K. Xiao, Q. Liu, G.H. Xie, P. Li, J. Ma, Y. Tian, L.P. Wen, L. Jiang, *J. Amer. Chem. Soc.* **2015**, *137*, 14765–14772.

[14] Z. Zhang, G.H. Xie, K. Xiao, X.-Y. Kong, P. Li, Y. Tian, L.P. Wen, L. Jiang, *Adv. Mater*. **2016**, *28*, 9613–9619.

[15] G.H. Xie, K. Xiao, Z. Zhang, X.-Y. Kong, Q. Liu, P. Li, L.P. Wen, L. Jiang, *Angew. Chem. Int. Ed*. **2015**, *54*, 13664–13668.

[16] D.P. He, E. Madrid, B.D.B. Aaronson, L. Fan, J. Doughty, K. Mathwig, A.M. Bond, N.B. McKeown, F. Marken, *ACS Appl. Mater. Interfaces* **2017**, *9*, 11272–11278.

[17] B.R. Putra, K.J. Aoki, J.Y. Chen, F. Marken, *Langmuir* **2019**, *35*, 2055–2065.

[18] H.J. Koo, O.D. Velev, *Biomicrofluidics* **2013**, *7*, 031501.

[19] H.G. Chun, T.D. Chung, *Ann. Rev. Anal. Chem.* **2015**, *8*, 441–462.

[20] B.R. Putra, M. Carta, R. Malpass-Evans, N.B. McKeown, F. Marken, *Electrochim. Acta* **2017**, *258*, 807–813.

[21] E. Madrid, P. Cottis, Y.Y. Rong, A.T. Rogers, J.M. Stone, R. Malpass-Evans, M. Carta, N.B. McKeown, F. Marken, *J. Mater. Chem. A* **2015**, *3*, 15849–15853.

[22] L. Tshwenya, O.A. Arotiba, B.R. Putra, E. Madrid, K. Mathwig, F. Marken, *J. Electroanal. Chem.* **2018**, *815*, 114–122.

[23] B.D.B. Aaronson, D. Wigmore, M.A. Johns, J.L. Scott, I. Polikarpov, F. Marken, *Analyst* **2017**, *142*, 3707–3714.

[24] B.R. Putra, C. Harito, D.V. Bavykin, F.C. Walsh, W. Tri Wahyuni, J.A. Boswell, A.M Squires, J.M.F. Schmitt, M. Alves Da Silva, K.J. Edler, P.J. Fletcher, A.E. Gesell, F. Marken, *J. Solid State Electrochem.* **2019**, 10.1007/s10008-019-04199-4.

[25] L. Rassaei, M. Sillanpaa, M.J. Bonne, F. Marken, *Electroanalysis* **2007**, *19*, 1461–1466.

[26] E. Azwar, W.A.W. Mahari, J.H. Chuah, D.V.N. Vo, N.L. Ma, W.H. Lam, S.S. Lam, *Internat. J. Hydrogen Energy* **2018**, *43*, 20811–20821.

[27] R.A. Webster, J.D. Watkins, R.J. Potter, F. Marken, *RSC Adv*. **2012**, *2*, 4886–4890.

[28] F. Marken, M.L. Gerrard, I.M. Mellor, R.J. Mortimer, C.E. Madden, S. Fletcher, K. Holt, J.S. Foord, R.H. Dahm, F. Page, *Electrochem. Commun.* **2001**, *3*, 177–180.

[29] A. Chinnappan, C. Baskar, S. Baskar, G. Ratheesh, S. Ramakrishna, *J. Mater. Chem. C* **2017**, *5*, 12657–12673.

[30] A.B. Suriani, A.R. Dalila, A. Mohamed, M.S. Rosmi, M.H. Mamat, M.F. Malek, M.K. Ahmad, N. Hashim, I.M. Isa, T. Soga, M. Tanemura, *Cogent Physics* **2016**, *3*, 1247486.

[31] S.Y. Zhao, J.N. Wang, X.Y. Du, J. Wang, R. Cao, Y.Y. Yin, X.L. Zhang, Z.Q. Yuan, Y. Xing, D.Y.H. Pui, C.J. Li, *ACS Appl. Energy Mater.* **2018**, *1*, 2326–2332.

[32] C. Yang, M.E. Denno, P. Pyakurel, B.J. Venton, *Anal. Chim. Acta* **2015**, *887*, 17-37.

[33] K. Lee, J.J. Zhang, H.J. Wang, D.P. Wilkinson, *J. Appl. Electrochem.* **2006**, *36*, 507–522.

[34] L.F. Chen, Y. Feng, H.W. Liang, Z.Y. Wu, S.H. Yu, *Adv. Energy Mater*. **2017**, *7*, 1700826.

[35] A. Mianowski, M. Owczarek, A. Marecka, *Iodine Energy Sources*, Part A, **2007**, *29*, 839–850.

[36] R.W. Ramette, R.W. Sandford, *J. Amer. Chem. Soc.* **1965**, *87*, 5001–5002.

[37] A.B. Suriani, A.R. Dalila, A. Mohamed, I.M. Isa, A. Kamari, N. Hashim, T. Soga, M. Tanemura, *Mater. Res. Bull.* **2015**, *70*, 524–529.